Footprints of a possible Ceres asteroid paleo-family

V Carruba, D. Nesvorný, S. Marchi, Safwan Aljbaae

Footprints of a possible Ceres asteroid paleo-family

V. Carruba,[1,2]★ D. Nesvorný,[2] S. Marchi[2] and S. Aljbaae[1]

[1]*UNESP, Univ. Estadual Paulista, Grupo de dinâmica Orbital e Planetologia, Guaratinguetá, SP, 12516-410, Brazil*
[2]*Department of Space Studies, Southwest Research Institute, Boulder, CO 80302, USA*

ABSTRACT

Ceres is the largest and most massive body in the asteroid main belt. Observational data from the Dawn spacecraft reveal the presence of at least two impact craters about 280 km in diameter on the Ceres surface, that could have expelled a significant number of fragments. Yet, standard techniques for identifying dynamical asteroid families have not detected any Ceres family. In this work, we argue that linear secular resonances with Ceres deplete the population of objects near Ceres. Also, because of the high escape velocity from Ceres, family members are expected to be very dispersed, with a considerable fraction of km-sized fragments that should be able to reach the pristine region of the main belt, the area between the 5J:-2A and 7J:-3A mean-motion resonances, where the observed number of asteroids is low. Rather than looking for possible Ceres family members near Ceres, here we propose to search in the pristine region. We identified 156 asteroids whose taxonomy, colours, albedo could be compatible with being fragments from Ceres. Remarkably, most of these objects have inclinations near that of Ceres itself.

Key words: celestial mechanics – minor planets, asteroids: general – minor planets, asteroids: individual: Ceres.

1 INTRODUCTION

Ceres is the largest and most massive body in the asteroid main belt. While many other large bodies of similar composition such as Pallas, Hygiea, Euphrosyne have asteroid families, no such group has been so far identified for Ceres (Milani et al. 2014; Nesvorny, Broz & Carruba 2015). Yet collisional models suggest that about 10 craters larger than 10 km in diameter should have formed over 4.55 Gyr of collisional evolution in the main belt (Marchi et al. 2016). Also, observational data from the Dawn probe show that at least two ≃280-km sized craters were formed in the last ≃2 Gyr on Ceres surface, and larger impacts may have happened in the past (Marchi et al. 2016). The absence of a Ceres family is therefore a major mystery in asteroid dynamics (Milani et al. 2014; Rivkin, Asphaug & Bottke 2014; Nesvorny, Broz & Carruba 2015). Previous works have suggested the possibility that the outer shell of Ceres could have been rich in ice, and that family members could have sublimated or been eroded by collisional evolution on time-scales of hundreds of millions of years (Rivkin et al. 2014). Alternatively, it has also been hypothesized that km-sized fragments ejected at Ceres escape velocity would likely disintegrate (Milani et al. 2014). Results from the Dawn mission set however an upper limit of 40 per cent in the ice content of Ceres outer shell (de Sanctis

et al. 2015; Fu et al. 2015), which seems too low to explain the lack of a family.

In this work we argue that the unique nature of Ceres as a dwarf planet may have indeed produced families not easily detectable using methods calibrated for smaller, less massive bodies. Close encounters and linear secular resonances with Ceres are expected to have significantly depleted the orbital region in the near proximity of this body, so reducing the number of the closest Ceres neighbours. More importantly, initial ejection velocities should have been significantly larger than those observed for any other parent body in the main belt, including Vesta, spreading the collision fragments in a much larger area. Members of the Ceres family would be significantly more distant among themselves than the typical distances between objects formed in collisions from smaller bodies, making an identification of the Ceres family quite challenging.

Rather than looking for members of a Ceres group in the central main belt, the region of the main belt with the highest concentration of asteroids, and where two other large Ch families, Dora and Chloris (Nesvorny et al. 2015) would make the taxonomical identification of former members of a Ceres family or paleo-family (an old dispersed family with an age between 2.7 and 3.8 Gyr, Carruba et al. 2015b) difficult, in this work we suggest to search for Ch-type objects in the pristine region of the main belt, between the 5J:-2A and 7J:-3A mean-motion resonances (or between 2.825 and 2.960 au in proper semimajor axis). This region of the asteroid belt was depleted of asteroids during the Late Heavy Bombardment (LHB hereafter) phase by sweeping mean-motion resonances, and the two
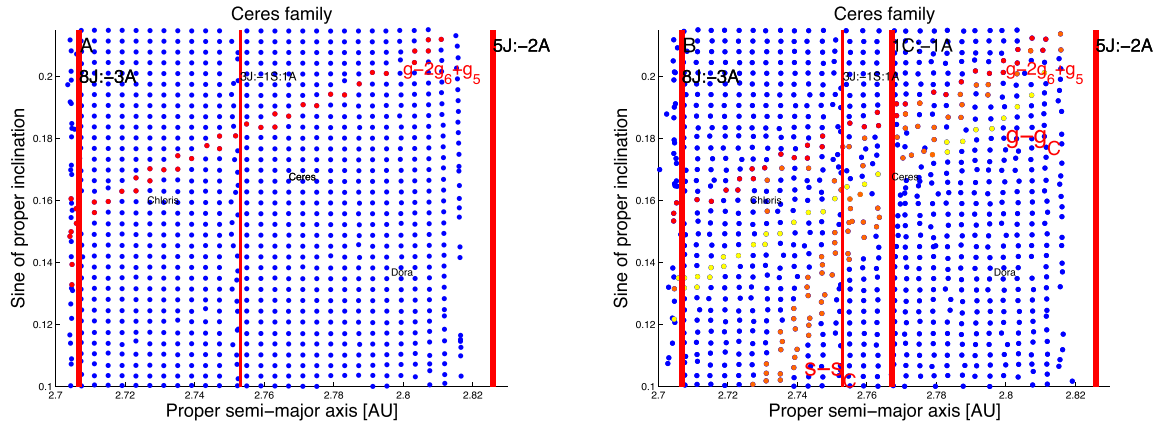
*E-mail: vcarruba@gmail.com

Figure 1. Dynamical maps for the orbital region of Ceres obtained by integrating test particles under the influence of all planets (panel A), and all planets and Ceres as a massive body (panel B). Unstable regions associated with mean-motion resonances appear as vertical strips. Secular resonance appear as inclined bands of aligned dots. Dynamically stable regions are shown as uniformly covered by blue dots. Vertical lines display the location of the main mean-motion resonances in the area. Red filled dots in both panels show the locations of 'likely resonators' in the $g - 2g_6 + g_5$ secular resonance. Yellow and orange filled dots in panel B show the orbital locations of likely resonators in the linear secular resonances with Ceres of pericentre and node, respectively. The orbital location of 1 Ceres, 668 Dora, and 410 Chloris are labelled.

mean-motion resonances with Jupiter have since limited the influx of outside material from other areas of the asteroid belt (Brož et al. 2013). The lower density of asteroids and the lack of other major C-type families at eccentricities and inclinations comparable to those of Ceres makes the identification of possible members of the Ceres family an easier task in this region. Identifying concentrations of C-type objects at values of inclinations comparable with that of Ceres itself could therefore be a strong circumstantial evidence about the formation of a Ceres family in the past.

2 EFFECTS OF LOCAL DYNAMICS

Ceres is the only dwarf planet in the asteroid belt. While its mass is not large enough to clear its orbital neighbourhood, significant dynamical perturbations are expected from this body, either as a consequence of close encounters (Carruba et al. 2003) or because of linear secular resonances involving the precession frequency of Ceres node s_C or pericentre g_C, and those of a given asteroid (Novaković et al. 2015). To investigate the importance of Ceres as a perturber, we obtain proper elements for 1400 particles in the plane of proper semimajor axis and inclination $(a, \sin(i))$, with the approach described in Carruba (2010), based on the method for obtaining synthetic proper elements of Knežević & Milani (2003). We integrated the particles over 20 Myr under the gravitation influence of (i) all planets and (ii) all planets plus Ceres as a massive body[1] with $SWIFT\_MVSF$, the symplectic integrator based on $SWIFT\_MVS$ from the *Swift* package of Levison & Duncan (1994), and modified by Brož (1999) to include online filtering of osculating elements. The initial osculating elements of the particles went from 2.696 to 2.832 au in a and from $5°.5$ to $13°.3$ in i. We used 35 intervals in a and 40 in i. The other orbital elements of the test particles were set equal to those of Ceres at the modified Julian date of 57 200.

Fig. 1 displays our results, as two dynamical maps. Each blue dot is associated with a particle proper $(a, \sin(i))$ value. For the case without Ceres as a massive body, displayed in panel A, the

orbital region near Ceres is relatively stable. The only important non-linear secular resonance in the region is the $g - 2g_6 + g_5$ (or $2\nu_6 - \nu_5$, in terms of linear secular resonances). Objects whose pericentre frequency is within ± 0.3 arcsec yr^{-1} from $2g_6 + g_5 = 52.229$ arcsec yr^{-1}, likely resonators in the terminology of Carruba (2009), are shown as red full dots in this figure. This is a diffusive secular resonance, and asteroids captured into this resonance may drift away, but will not be destabilize (Carruba et al. 2014). The situation is much different and more interesting for the map with Ceres as a massive body.

As observed in Fig. 1, panel B, accounting for Ceres causes the appearance of a 1:1 mean-motion resonance with this dwarf planet. Most importantly, linear secular resonances of nodes $s - s_C$ and pericentre $g - g_C$, first detected by Novaković et al. (2015) significantly destabilize the orbits in the proximity of Ceres. Combined with the long-term effect of close encounters with Ceres, this has interesting consequences for the survival of members of the Ceres family in the central main belt. Not many family members are expected to survive near Ceres, and this would cause significant difficulties in using standard dynamical family identification techniques, since they are based on looking for pairs of neighbours in proper element domains (Hierarchical Clustering Method, HCM hereafter, Bendjoya & Zappalá 2002). Since the close neighbours of Ceres would have been removed on a short time-scale, only objects whose distance from Ceres is higher than the average distance between pairs of asteroids in the central main belt would have survived. Also, the area at higher inclination than that associated with the linear secular resonances with Ceres should be significantly depleted of asteroids, and this is actually observed (see for instance fig. 9 in Nesvorny et al. 2015). Finally, the Dora family, a large ($\simeq 1260$ members, Nesvorny et al. 2015) group of the same spectral type of Ceres, Ch, is located at lower inclinations than that of Ceres. Considering that the large Ch Chloris family is also encountered in the central main belt near Ceres, discriminating between a Ch asteroid from Ceres and one from Dora, Chloris, or other local sources would be a very daunting task, also considering that there are currently no identified members of a Ceres family that could serve as a basis for a taxonomical analysis.

To further investigate the efficiency of Ceres in perturbing its most immediate neighbours, we also performed numerical

---

[1] The mass of Ceres was assumed to be equal to 9.39×10^{20} kg, as determined by the Dawn spacecraft (Russell et al. 2015).
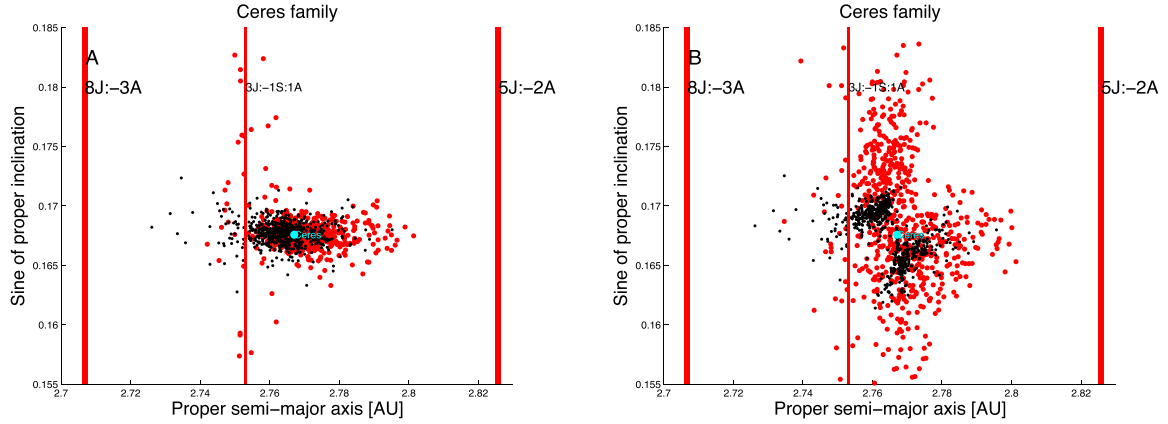
Figure 2. Projection in the proper $(a, \sin(i))$ plane of the initial (black full dots, $T = 1.2$ My) and final (red full dots, $T = 455.6$ My) elements of the simulated Ceres family members integrated under the gravitational influence of all planets (panel A), and all planets plus Ceres (panel B). Vertical lines display the location of the mean-motion resonances, the cyan full dot identify the orbital location of Ceres itself.

simulations of a fictitious Ceres family with the *SYSYCE* integrator (Swift+Yarkovsky+Stochastic YORP+Close encounters) of Carruba et al. (2015a), modified to also account for past changes in the values of the solar luminosity. This integrators accounts for both the diurnal and seasonal version of the Yarkovsky effect, the stochastic version of the YORP effect, and close encounters of massless particles with massive bodies. The numerical setup of our simulations was similar to what discussed in Carruba et al. (2015a): we used the optimal values of the Yarkovsky parameters discussed in Brož et al. (2013) for C-type asteroids, the initial spin obliquity was random, and normal reorientation time-scales due to possible collisions as described in Brož (1999) were considered for all runs. We integrated our test particles under the influence of all planets (case A), and all planets plus Ceres (case B), and obtained synthetic proper elements with the approach described in Carruba (2010).

The fictitious Ceres family was generated with the approach described in Vokrouhlický et al. (2006): we assumed that the initial ejection velocity field follows an isotropical Gaussian distribution of zero mean and standard deviation given by

$$\sigma_{V_{ej}} = V_{EJ} \left(\frac{5 \text{km}}{D} \right), \qquad (1)$$

where D is the body diameter in km, and V_{EJ} is a parameter describing the width of the velocity field. We used the relatively small value of $V_{EJ} = 60 \text{ m s}^{-1}$ for our simulated family. In the next section we will discuss why it is quite likely that any possible Ceres family would have a much larger value of V_{EJ}. Since here, however, we were interested in the dynamics in the proximity of Ceres itself, our choice of V_{EJ} was, in our opinion, justified. We generated 642 particles with size-frequency distributions (SFD) with an exponent $-\alpha$ that best fitted the cumulative distribution equal to 3.6, a fairly typical value (Masiero et al. 2012), and with diameters in the range from 2.0 to 12.0 km.

Fig. 2 displays our results in the proper $(a, \sin(i))$ plane for the simulation without Ceres as a massive body (panel A) and with a massive Ceres (panel B). Black full dots display the position of simulated Ceres family members at the beginning of the simulation, after 1.2 My, while the red full dots show the orbital location at the end of the integration, for $T = 455.6$ My. For the case without Ceres one can notice that the family does not disperse much, and that most of the scattering is caused by the 3J:-1S:1A three-body resonance. Results including Ceres as a perturber are quite more interesting: already after just 1.2 My secular resonances with Ceres cleared a

gap near the orbital location of the dwarf planet, identified by a full blue dot. The situation is even more dramatic at the end of the simulation, where we observe that Ceres scattered material at lower and higher inclinations with respect to the case in which Ceres had no mass, and opened a significant gap at the family centre, as also observed in the dynamical map of Fig. 1, panel B.

How difficult would be to identify our simulated Ceres family using HCM? To answer this question, we computed the nominal distance velocity cutoff d_0 for which two nearby asteroids are considered to be related using the approach of Beaugé & Roig (2001), that defines this quantity as the average minimum distance between all possible asteroid pairs, as a function of time, for (i) all paired asteroids in the simulated Ceres family (d_0), and (ii) just with respect to Ceres itself (d_{Ceres}). This latter quantity provides an estimate of the minimum value of distance cutoff needed to identify a Ceres family using the standard HCM. The maximum value of the nominal distance velocity cutoff for the simulated Ceres family was equal to 17.7 m s^{-1}. When Ceres was not considered as a massive body, values of d_{Ceres} were of the order of 5 m s^{-1}, at all times below the nominal distance velocity cutoff (see Fig. 3, blue line). Once Ceres was included as a massive body, however, values of d_{Ceres} quickly surpassed the nominal distance velocity cutoff d_0 (see red line in Fig. 3): after 200 My, except of short episodes in which $d_{Ceres} < d_0$, for most of the time d_{Ceres} was larger than d_0. After 380 My, this trend was consolidated and d_{Ceres} was always larger than d_0. The identification of a Ceres family using HCM in the domain of proper elements of the simulated family and Ceres as the first body would be quite challenging after 380 My.

So, where to look for hypothetical surviving members of a Ceres family? The next section will be dealing with estimating the extent of the initial orbital dispersion of a putative family, and in assessing the regions where locating its members could be easier.

3 EJECTION VELOCITIES OF A POSSIBLE CERES FAMILY

The escape velocity V_{esc} from Ceres is considerably larger than that of other, less massive bodies: $\simeq$480 m s^{-1} (Russell et al. 2015) versus the 360 m s^{-1} for Vesta (Russell et al. 2012), the largest body in the main belt with a uncontroversial recognized asteroid family. The Vesta family is one of the largest in the main belt, and one would expect a putative Ceres family to be even larger.
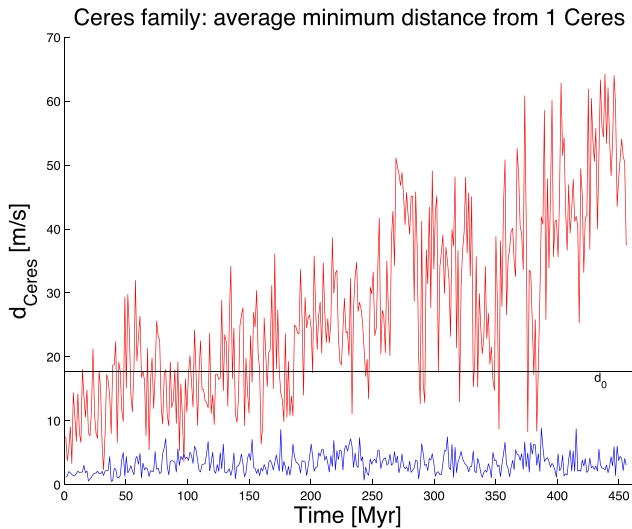
Figure 3. Averaged minimum distance from Ceres d_{Ceres} as a function of time of the simulated family members for the case without (blue line) and with (red line) Ceres as a massive body. The horizontal black line displays the maximum nominal distance cutoff level d_0 for the whole simulated Ceres family.

Recently, Carruba & Nesvorný (2016) investigated the shape of the ejection velocity field of 49 asteroid families. Typical observed values of $\beta = V_{\text{EJ}}/V_{\text{esc}}$, with V_{EJ} given by equation (1), are between 0.5 and 1.5 (see also Nesvorny et al. 2015, section 5).[2] While for typical asteroid families this implies that V_{EJ} is generally lower than 100 m s^{-1}, even a conservative choice of $\beta = 0.5$ for Ceres would produce a field with V_{EJ} of the order of 240 m s^{-1}. This is more than a factor of 2 larger than the higher values of V_{EJ} observed for some of the oldest asteroid families (Carruba et al. 2015b), but not inconsistent with the observed presence of crater ray systems around large craters on Ceres, such as Occator (Nathues et al. 2015), that cover a large portion of the Ceres surface. Since the circular velocity needed to form such rays is of the order of half the escape velocity from Ceres, this suggests that values of β near 0.5 for the V_{EJ} parameter of a possible Ceres family are not unreasonable. Following the approach of Vokrouhlický et al. (2006), see also Carruba et al. (2015b), we generated fictitious Ceres asteroids members with diameters 1, 3, and 7 km with the minimum and maximum value of β from Carruba & Nesvorný (2016).

Fig. 4 displays our results for $\beta = 0.2$ (panel A) and $\beta = 1.5$ (panel B). Even in the most conservative case of $\beta = 0.2$, a value lower than those of any of the families studied in Carruba & Nesvorný (2016), we still found that a significative fraction[3] of the

multi-km (and potentially observable) fragments from Ceres could have been injected in the pristine region of the main belt. We define this region as the area between the 5J:-2A and 7J:-3A mean-motion resonances with Jupiter. Because of these two dynamical barriers, very little material from external regions can reach this area (Brož et al. 2013). As a consequence, the local density of asteroids is much inferior to that of other regions of the asteroid belt. Also, only small C-type families, such those of Naema (301 members), Terpsichore (138 members), and Terentia (79 members) (Nesvorny et al. 2015) are found in the region, and at eccentricity values quite different than that of Ceres, so easily distinguishable from putative Ceres fragments. If any large ($D > 5$ km), not easily movable by non-gravitation effects, members of a hypothetical Ceres family[4] would have been injected in this region after the LHB, it would be reasonable to expect that they could have remained there and still be visible today. We selected a region in the pristine zone where most of the $D > 1$ km objects could be found, according to our results for the most conservative case with $\beta = 0.2$ (black box in Fig. 4, panels A, this also corresponds to the region in which most of the $D > 3$ km objects would be located in the most optimistic scenario of $\beta = 1.5$, see black box in Fig. 4, panels B. In the next section we will investigate if any such object could be identified in the pristine region.

4 THE PRISTINE REGION

Results of a dynamical map with Ceres as a massive body, not shown for the sake of brevity, demonstrate that the pristine region at inclination close to that of Ceres is dynamically stable, with no linear secular resonances with Ceres and only minor diffusive secular resonances with the giant planets. In the black region of Fig. 4 there are four Ch asteroids, according to data from the three major photometric/spectroscopic surveys (ECAS (Eight-Colour Asteroid Analysis, Tholen et al. 1989), SMASS (Small Main Belt Spectroscopic Survey, Bus & Binzel 2002a,b), and S3OS2 (Small Solar System Objects Spectroscopic Survey, Lazzaro et al. 2004): 195 Eurykleia, 238 Hypatia, 910 Annelise, and 1189 Terentia. The *WISE* survey (Masiero et al. 2012) estimates that these objects have diameters of 85.7, 148.5. 47.1, and 55.9 km, respectively. With the possible and very doubtful exception of Annelise and Terentia, the other objects are too big to be realistically assumed to be members of a Ceres family. Apart from a small family of 79 members around Terentia (Nesvorny et al. 2015), no major family has been identified around the largest objects, that appear to be isolated. To increase statistics, we turn our attention to photometric data from the Sloan Digital Sky Survey-Moving Object Catalog data, fourth release (SDSS-MOC4 hereafter, Ivezić et al. 2001). Using the classification method of De-Meo & Carry (2013) in the *gri* slope and $z' - i'$ colours domain, we identified 23 C-type photometric candidates in the pristine region.

Fig. 5, panel A shows their orbital location in the $(a, \sin(i))$ plane. Vertical red lines display the orbital location of the main mean-motion resonances in the region, including the 2J:1S:-1A three-body resonance that divides the pristine area in two parts. 14 of the 23 SDSS C-type asteroids, 60.9 per cent of the total, can be found in the black region where we would expect Ceres family members to be located. By contrast, only six objects can be

---

[2] Isotropical ejection velocity field would be expected for large basins, as observed for the Vestoids. Cratering events, however may produce asymmetrical initial velocity field (Marchi et al. 2001; Novaković et al. 2012), and depending on the orbital configuration of Ceres at the time of the family formation event, namely, its values of true anomaly f and argument of pericentre ω, and on the impact geometry, family members may have not reached the pristine region. For simplicity, in this work we concentrated our analysis on large basins forming events. However, since collisional models predict that about 10 400 km or larger craters could have formed on Ceres (Marchi et al. 2016), we expect that, at least for a fraction of these events, some of the ejected material was likely to have reached the pristine region.
[3] 34.2, 10.6, and 0.5 per cent of the $D = 1$, 3, and 7 km populations, respectively.

[4] The LHB likely occurred 4.1–4.2 Gyr ago (e.g. Marchi et al. 2013), no family is expected to have survived this event, and we also expect he original population of asteroids in the pristine region to have been significantly depleted (Brasil et al. 2015).
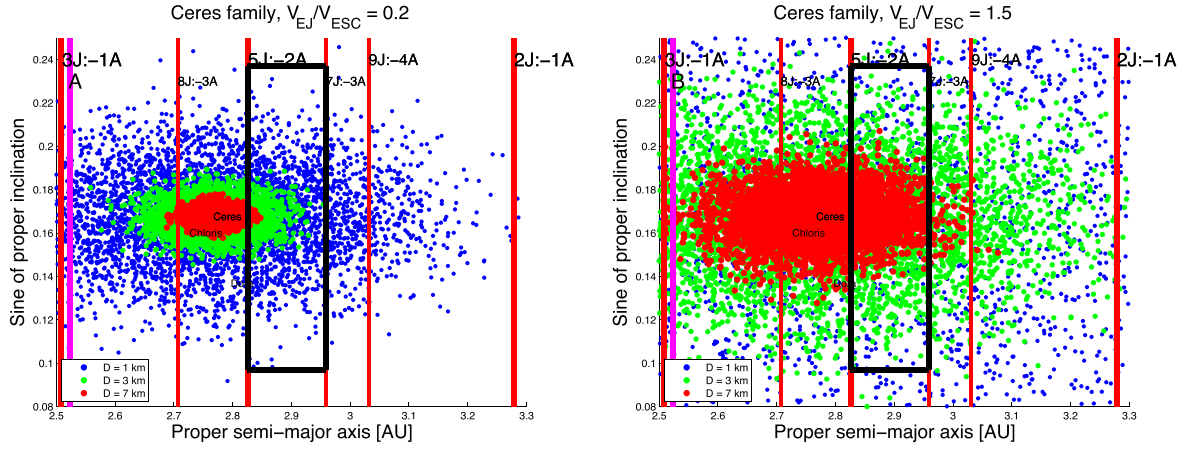
Figure 4. An (*a*, *sin(i)*) distribution of *D* = 1, 3, and 7 km members of Ceres families obtained using $V_{EJ} = 0.2 V_{ESC}$ (panel A) and $V_{EJ} = 1.5 V_{ESC}$ (panel B). The black box identify the orbital regions in which most of the *D* = 3 km fragments for $V_{EJ} = 1.5 \cdot V_{ESC}$ and most of the *D* = 1 km for $V_{EJ} = 0.2 \cdot V_{ESC}$ could be found in the pristine region of the main belt.
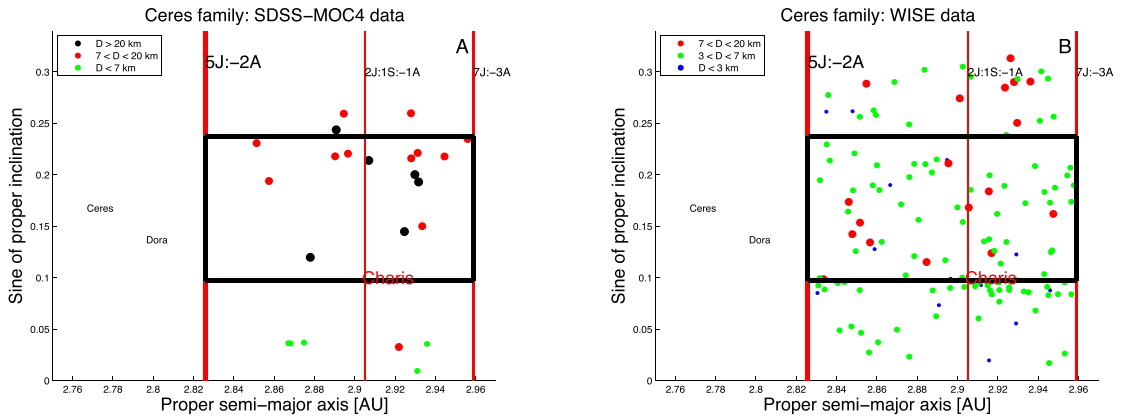

Figure 5. An (*a*, sin (*i*)) projection of 23 C-type SDSS-MOC4 photometric candidates (panel A) and 130 objects with *WISE* albedo in the range from 0.08 to 0.10 (panel B) in the pristine region. Candidates of different diameters are shown with the colour code reported in the figure legend. The orbital location of 627 Charis is identified by its name, in red letters.

found at lower inclinations, and only 3 at higher values. Overall, C-type photometric candidates in the pristine region tend to cluster at inclination values close to that of Ceres.

To check the statistical significance of this result, we checked what would be the probability that these 14 asteroids were produced by a fluctuation of a Poisson distribution (it has been suggested that the orbital distribution of background asteroids follows a Poisson distribution (Carruba & Machuca 2011)). Following the approach of Carruba & Machuca (2011), the probability that the expected number of *k* = 14 occurrences in a given interval is produced by the Poissonian statistics is given by

$$f(k, \lambda) = \frac{\lambda^k e^{-\lambda}}{k!}, \qquad (2)$$

where λ is a positive real number, equal to the expected number of occurrences in the given interval. Here we used for λ the number of SDSS candidates in the black region ($N_{SDSS} = 14$), weighted to account for the volume occupied by the region (V_{Reg}) with respect to the total volume considered in our analysis (V_{Tot}, we considered asteroids with sin (*i*) < 0.35). This is given by

$$\lambda = N_{SDSS} \frac{V_{Reg}}{V_{Tot}}, \qquad (3)$$

For our considered black region, this yield λ = 5.6, that corresponds to a probability to observe 14 bodies of just 0.13 per cent, quite less than the null hypothesis level of 1.0 per cent of the data being drawn from the Poisson distribution. Similar analysis performed for uniform and Gaussian distributions (see Carruba & Machuca 2011 for details on the procedures) also failed to fulfill the null hypothesis, which suggests that the observed concentration of asteroids at inclinations close to those of Ceres should be statistically significant.

To increase the number of possible Ceres members, we also look for objects in the *WISE* data base whose geometric albedo p_V is between 0.08 and 0.10, the range of albedo values observed for more than 90 per cent of the surface material at Ceres by the Dawn spacecraft (Li et al. 2015). While C-type objects with these values of *WISE* albedo could be associated with a Ceres family, other spectral types such as X, D, L, K, and even some S also have albedo values in this range, so this data must be considered with some caution. Nevertheless, it provides useful preliminary information. After eliminating objects belonging to spectral types other than C (13 bodies), members of the Terpsichore and Terentia families (7 asteroids), and of the X-type group Charis (5 objects), we were left with a sample of 130 asteroids in that range of albedos. The fact
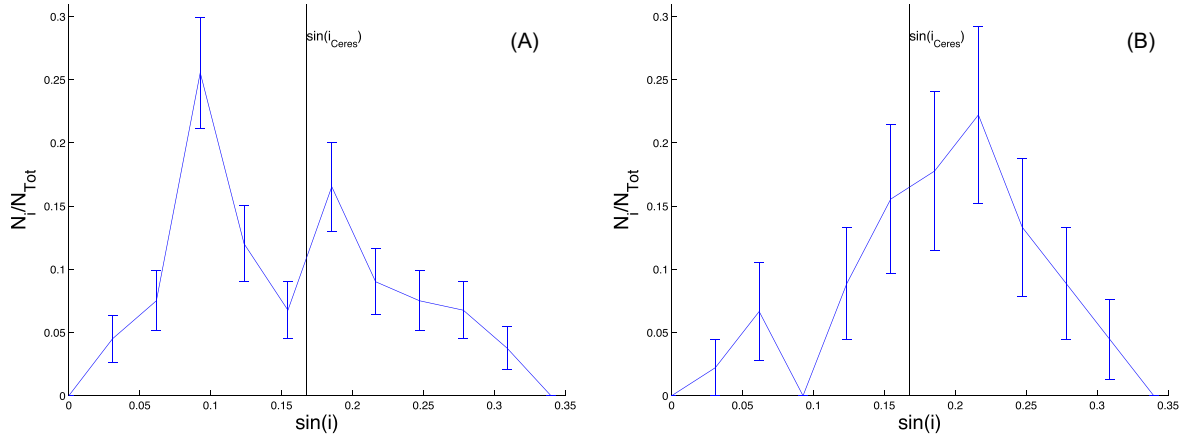
Figure 6. A histogram of the distribution of $\sin(i)$ values for 133 and 45 C-type (panels A and B, respectively) albedo candidates in the pristine region. The vertical line marks the value of Ceres inclination. Errors are assumed to be proportional to the square root of the number of asteroids in each size bin.

that only four C-type candidates were members of the Terpsichore family, and three of Terentia, 3.2 per cent of the total, seems to indicate that local sources may not explain all the local population of C-type candidates. Since the other C-type objects in the region have diameters less than that of Terpsichore, even if they produced families in the past (of which there is no trace today), we would expect that to account at most for 10 per cent of the observed population of C-type candidates.

Fig. 5, panel B, displays the $(a, \sin(i))$ distribution of these objects. Again, 67 asteroids, 51.5 per cent of the total, are found in the black region, while 39, (30.0 per cent) are found at lower inclinations and 24 (18.5 per cent) at higher i. 22 of the objects at low inclinations cluster near the X-type family Charis, and could quite possibly be associated with its halo. If we eliminate these objects, then the percentage of albedo candidates in the black region increase to 56.0 per cent, a result similar to that from the SDSS-MOC4 data. To reduce possible contaminations from the local large families of Charis, Eos and Koronis, which could have small populations of objects with *WISE* albedos in the studied range, we eliminated objects (i) with a beyond the 2J:1S:-1A mean-motion resonance that could potentially be associated with the Charis and Eos halo (Brož & Morbidelli 2013), and are less likely to have been produced by collisions on Ceres with low values of β, and (ii) those objects between the 5J:-2A and the 2J:1S:-1A mean-motion resonances with proper eccentricities lower than 0.08 and sine of proper inclinations lower than 0.06, that could potentially be members of the Koronis halo (Carruba, Nesvorný & Aljbaae 2016).

Fig. 6 shows a histogram of all the 133 C-type albedo candidates in the pristine region (panel A), and of the 45 asteroids that satisfied our criteria (panel B). In the first panel one can notice a peak at $\sin(i) \simeq 0.10$ associated with the local Charis X-type family, that is not visible once objects in the Charis halo are removed (panel B). Remarkably, there is a peak in the $\sin(i)$ distribution that nearly coincides with the current value of the inclination of Ceres. To check for its statistical significance, and in particular if it could be the product of fluctuations in a Poisson probability distribution, we used the approach described in Carruba & Machuca (2011), Section 4.1. For the N_i values of the number of asteroids per size bin in the histogram shown in Fig. 6, panel B, we best fitted the value of λ in equation (2) using the *MATLAB* routine (where *MATLAB* stands for Matrix Laboratory) *poissfit*. We then generated 1000 random populations of asteroids following the Poisson distribution with the routine *poissrnd*, and then

performed a Pearson χ^2 test by computing the χ^2-like variable defined as

$$\chi^2 = \sum_{i=1}^{n_{\text{int}}} \frac{(q_i - p_i)^2}{q_i}, \qquad (4)$$

where n_{int} is the number of intervals used in the histogram in Fig. 6, panel B with a number of objects larger than 0 (9), q_i is the number of real objects in the ith interval, and p_i is the number of simulated asteroids in the same $\sin(i)$ range. Assuming that the χ^2-like variable follows an incomplete gamma function probability distribution, the probability of the two distributions being compatible can be computed considering the minimum value of χ^2 (17.46, in our case) and the number of degrees of freedom (9, Press 2001). This yields a probability of 0.8 per cent of the two distributions being compatible, below the null hypothesis, which implies that the observed peak should be statistically significant. Similar results were obtained for the uniform and Gaussian distributions.

While not a conclusive proof of the possible existence of a Ceres family, this interesting result represents, in our opinion, a circumstantial evidence in favour of this possibility. A list of the photometric and albedo Ceres members candidates with diameters less than 20 km in the pristine region identified in this work is provided in Table 1.

5 CONCLUSIONS

Our results could be summarized as follows.

(i) We studied the effect that the local dynamics may have had on a possible Ceres family in the central main belt. Resonances with Ceres would have depleted the population of members at higher inclinations than Ceres itself, and close encounters with the dwarf planet would also caused further spread of the family, making the identification of a Ceres dynamical group impossible after timescales of 200–400 My. Members of the Ceres family at low inclinations would not be easily distinguishable from members of other local large Ch families such as Dora and Chloris.

(ii) We investigated the original spread that a Ceres family may have had in the $(a, e, \sin(i))$ proper element domain. Assuming that values of the initial ejection velocity parameter $\beta = V_{\text{EJ}}/V_{\text{esc}}$, would be in the range observed for other families, we expect that a potentially observable population of $D > 3$ km fragments,

Table 1. Photometric and albedo Ceres family candidates in the pristine region with $D < 20$ km. We report the asteroid identification, its proper a, e, sin (i), its absolute magnitude H, the estimated diameter D, and if it is a photometric (SDSS) or an albedo (*WISE*) C-type candidate. Asteroids in the expected inclination range of the Ceres family are marked with a dagger (†). The 45 asteroids that satisfied our selection criteria for Fig. 6, panel B, have their identifications marked in bold.

Identification	Semimajor axis (au)	Eccentricity	Sine of inclination	Absolute magnitude	Diameter (km)	Type
2082	2.921 907	0.193 664	0.032 701	13.30	17.12	SDSS
5994 (†)	2.851 295	0.184 111	0.230 810	11.98	17.80	SDSS
6671	2.894 602	0.135 151	0.259 412	12.54	13.75	SDSS
6721	2.928 060	0.160 947	0.290 183	12.40	14.93	*WISE*
8560 (†)	2.956 013	0.055 937	0.234 792	12.30	18.95	SDSS
8706 (†)	2.847 802	0.081 223	0.142 328	13.30	9.59	*WISE*
11771 (†)	2.916 868	0.182 122	0.123 918	13.90	7.60	*WISE*
12356	2.935 904	0.069 843	0.035 674	13.10	6.01	SDSS
12986 (†)	2.930 536	0.071 421	0.192 957	13.90	7.77	*WISE*
14037 (†)	2.846 048	0.113 655	0.173 687	12.80	12.86	*WISE*
14338 (†)	2.944 557	0.079 173	0.217 839	12.40	8.99	SDSS
14531 (†)	2.833 541	0.136 888	0.098 603	13.80	8.12	*WISE*
16885 (†)	2.890 294	0.089 698	0.218 012	12.90	15.54	SDSS
18198 (†)	2.928 039	0.165 372	0.216 076	13.60	9.67	SDSS
18463	2.856 107	0.121 585	0.027 381	14.40	5.89	*WISE*
20094 (†)	2.861 264	0.126 932	0.185 285	14.40	6.16	*WISE*
20095	2.867 089	0.044 780	0.036 435	14.44	5.73	SDSS
20965 (†)	2.929 609	0.106 764	0.250 502	13.20	10.62	*WISE*
21714 (†)	2.896 649	0.056 614	0.220 559	12.50	8.27	SDSS
22540	2.874 836	0.064 495	0.036 984	14.00	3.60	SDSS
23000 (†)	2.931 225	0.042 298	0.221 314	13.90	14.06	SDSS
23136	2.927 916	0.115 123	0.259 867	13.50	8.05	SDSS
23432	2.910 407	0.099 806	0.060 429	15.00	4.32	*WISE*
26085	2.847 349	0.071 938	0.052 672	14.20	6.12	*WISE*
28297 (†)	2.933 505	0.149 849	0.150 057	13.60	9.36	SDSS
29514	2.936 161	0.193 732	0.290 663	13.20	10.40	*WISE*
29906 (†)	2.884 096	0.043 687	0.210 437	14.00	6.84	*WISE*
31232 (†)	2.857 460	0.055 909	0.194 055	14.40	7.27	SDSS
32421 (†)	2.915 570	0.131 466	0.183 926	13.70	8.45	*WISE*
32586 (†)	2.905 601	0.142687	0.168 171	12.80	11.24	*WISE*
33202	2.931 046	0.058 748	0.009 448	14.46	5.68	SDSS
34129	2.868 182	0.042 556	0.036 113	15.00	4.11	SDSS
35533 (†)	2.902 357	0.098 794	0.100 204	14.50	5.91	*WISE*
38466	2.860 576	0.046 388	0.037 292	15.10	4.09	*WISE*
42544	2.914 965	0.087 749	0.092 480	14.70	4.85	*WISE*
42710 (†)	2.939 916	0.070 241	0.191 939	13.90	7.49	*WISE*
43235 (†)	2.835 135	0.069 649	0.229 597	14.00	6.72	*WISE*
44357	2.938 663	0.176 620	0.068 078	14.50	5.65	*WISE*
46645	2.944 500	0.159 099	0.091 087	14.00	6.97	*WISE*
47651 (†)	2.836 642	0.070 337	0.213 856	14.60	5.36	*WISE*
47862 (†)	2.887 313	0.087 727	0.202 313	14.30	6.29	*WISE*
51050 (†)	2.876 180	0.169 556	0.197 835	14.00	6.87	*WISE*
51338 (†)	2.947 534	0.178 943	0.161 967	13.10	11.14	*WISE*
51707 (†)	2.893 943	0.194 367	0.117 033	14.50	5.82	*WISE*
53875 (†)	2.895 506	0.046 369	0.211 182	13.70	8.32	*WISE*
54065 (†)	2.948 372	0.120 630	0.187 491	15.00	4.25	*WISE*
54930 (†)	2.915 907	0.102 511	0.199 583	14.90	4.42	*WISE*
54966 (†)	2.928 465	0.101 667	0.098 231	14.50	5.30	*WISE*
55903	2.941 553	0.124 014	0.300 482	14.50	5.68	*WISE*
57676	2.840 613	0.081 003	0.094 847	15.40	3.51	*WISE*
57695	2.953 239	0.067 685	0.026 310	15.20	4.28	*WISE*
61674 (†)	2.856 602	0.145 630	0.134 328	13.70	8.21	*WISE*
65774	2.876 079	0.084 274	0.023 299	15.40	3.89	*WISE*
66046	2.923 553	0.054 957	0.284 802	13.80	7.83	*WISE*
66648 (†)	2.857 988	0.126 132	0.189 854	15.50	3.57	*WISE*
67333 (†)	2.884 682	0.186 828	0.115 222	14.00	7.41	*WISE*
71263 (†)	2.851 656	0.166 470	0.153 571	13.90	7.29	*WISE*
72691 (†)	2.954 464	0.092 571	0.199 377	14.40	5.88	*WISE*
74398	2.926 309	0.113 313	0.313 344	13.20	9.78	*WISE*
76814	2.854 806	0.079 048	0.288 523	13.90	7.56	*WISE*
77346	2.925 627	0.114 702	0.090 742	15.30	3.93	*WISE*

Table 1 – *continued*

Identification	Semimajor axis (au)	Eccentricity	Sine of inclination	Absolute magnitude	Diameter (km)	Type
77873 (†)	2.943 052	0.183 550	0.103 473	14.10	6.63	WISE
82715 (†)	2.831 806	0.085 409	0.194 841	13.90	6.99	WISE
82897 (†)	2.878 531	0.056 788	0.210 677	14.50	5.69	WISE
83337 (†)	2.831 666	0.098 578	0.099 738	14.30	6.24	WISE
83707	2.830 936	0.085 110	0.092 492	14.00	6.80	WISE
85114	2.835 897	0.132 118	0.277 561	15.10	4.20	WISE
88573 (†)	2.919 644	0.132 783	0.162 074	14.40	5.92	WISE
88723	2.834 080	0.088 113	0.088 653	14.90	4.69	WISE
89727	2.945 443	0.101 456	0.017 127	15.40	3.75	WISE
91870 (†)	2.845 707	0.116 806	0.164 315	14.70	5.11	WISE
91997 (†)	2.921 480	0.078 832	0.113 695	14.80	5.09	WISE
97020	2.901 140	0.058 409	0.274 274	14.10	7.04	WISE
103529	2.920 771	0.052 655	0.088 095	15.50	3.36	WISE
103923 (†)	2.933 675	0.076 817	0.172 426	15.40	3.61	WISE
104028 (†)	2.923 278	0.054 426	0.189 286	14.60	5.39	WISE
105129 (†)	2.862 443	0.199 475	0.134 897	15.00	4.70	WISE
108386 (†)	2.956 425	0.080 106	0.173 829	15.20	4.10	WISE
111331	2.917 046	0.091 109	0.083 911	15.20	4.21	WISE
111394 (†)	2.946 302	0.090 717	0.124 884	14.50	5.73	WISE
112976 (†)	2.878 561	0.086 200	0.121 019	14.90	4.56	WISE
113564	2.851 523	0.085 304	0.087 892	14.80	4.78	WISE
119722	2.852 195	0.072 637	0.046 523	15.30	3.92	WISE
120043 (†)	2.927 114	0.071 038	0.193 386	14.60	5.40	WISE
121281	2.844 024	0.150 695	0.095 594	15.00	4.65	WISE
125857	2.896 361	0.102 890	0.090 084	15.70	3.28	WISE
128714	2.868 729	0.041 501	0.290 199	14.40	5.81	WISE
129048 (†)	2.848 874	0.132 366	0.220 818	14.90	4.71	WISE
130023 (†)	2.880 666	0.139 291	0.156 271	14.80	5.14	WISE
131267 (†)	2.848 184	0.130 562	0.184 916	14.90	4.57	WISE
133841	2.932 969	0.065 715	0.086 641	14.90	4.47	WISE
139184 (†)	2.915 685	0.191 200	0.137 376	15.60	3.20	WISE
139793	2.953 216	0.076 844	0.095 644	15.30	3.72	WISE
140007	2.841 540	0.052 047	0.048 892	14.60	5.45	WISE
140769 (†)	2.860 013	0.068 603	0.209 332	15.20	4.21	WISE
143166	2.869 961	0.101 913	0.049 494	15.30	3.81	WISE
144712 (†)	2.915 620	0.171 867	0.019 665	15.90	2.85	WISE
144715 (†)	2.872 016	0.110 133	0.171 309	15.40	3.73	WISE
145325 (†)	2.849 511	0.122 737	0.125 786	15.20	4.14	WISE
145392	2.902 675	0.059 978	0.305 121	14.80	5.07	WISE
155547	2.935 295	0.076 924	0.086 005	15.30	3.88	WISE
159263	2.851 540	0.121 195	0.256 403	15.40	3.66	WISE
166760	2.945 129	0.099 172	0.082 949	15.00	4.22	WISE
169161	2.889 445	0.116 778	0.062 533	15.90	3.04	WISE
172377 (†)	2.902 666	0.179 680	0.154 193	14.80	4.62	WISE
174489	2.929 807	0.132 278	0.293 032	14.90	4.48	WISE
176347 (†)	2.918 230	0.086 535	0.126 204	14.80	4.77	WISE
178669	2.956 492	0.110 930	0.083 905	15.50	3.57	WISE
181605 (†)	2.874 33	0 0.15 8614	0.102 414	15.30	4.01	WISE
182687	2.910 644	0.119 178	0.095 378	15.50	3.38	WISE
184356	2.908 767	0.107 959	0.091 759	15.50	3.43	WISE
184487	2.945 952	0.095 575	0.087 735	16.10	2.61	WISE
189495	2.944 911	0.133 490	0.293 474	14.30	6.32	WISE
191486	2.947 722	0.145 902	0.256 494	14.60	5.36	WISE
192044	2.940 902	0.074 702	0.252 544	14.70	5.04	WISE
197144	2.925 675	0.105 006	0.088 102	15.00	4.34	WISE
198403 (†)	2.906 537	0.088 144	0.185 480	15.50	3.37	WISE
198808 (†)	2.924 283	0.073 838	0.238 708	14.60	5.27	WISE
201824	2.876 024	0.082 627	0.248 968	14.90	4.54	WISE
214826	2.949 845	0.113 408	0.084 030	15.80	3.03	WISE
218273	2.887 695	0.078 069	0.087 647	15.50	3.70	WISE
218776 (†)	2.924 260	0.057 623	0.134 816	15.60	3.38	WISE
222080 (†)	2.866 610	0.149 922	0.190 036	16.10	2.68	WISE
227004 (†)	2.913 158	0.058 757	0.135 286	15.20	3.93	WISE
231791 (†)	2.889 728	0.157 418	0.214 961	14.90	4.84	WISE

Table 1 – *continued*

Identification	Semimajor axis (au)	Eccentricity	Sine of inclination	Absolute magnitude	Diameter (km)	Type
232724	2.903 389	0.120 023	0.091 075	15.50	3.66	*WISE*
235975	2.920 486	0.101 497	0.095 416	15.30	3.77	*WISE*
236004 (†)	2.943 159	0.076 640	0.183 347	15.30	3.67	*WISE*
238734 (†)	2.957 799	0.056 591	0.189 721	15.60	3.26	*WISE*
239518	2.859 584	0.120 313	0.258 105	15.40	3.50	*WISE*
239993 (†)	2.955 953	0.053 980	0.206 900	15.20	3.98	*WISE*
240384	2.834 916	0.123 127	0.261 325	16.30	2.45	*WISE*
243283	2.890 796	0.122 268	0.073 358	16.40	2.45	*WISE*
243302 (†)	2.938 414	0.125 304	0.208 466	15.90	3.06	*WISE*
243774	2.906 543	0.130 365	0.295 275	14.90	4.43	*WISE*
243854 (†)	2.947 074	0.198 642	0.126 632	15.70	3.30	*WISE*
244955 (†)	2.899 970	0.057 671	0.168 345	15.50	3.50	*WISE*
245480	2.858 417	0.093 258	0.262 532	15.60	3.50	*WISE*
246409	2.929 076	0.145 512	0.055 515	15.90	2.84	*WISE*
246466	2.830 511	0.084 131	0.085 150	16.10	2.64	*WISE*
246720	2.911 652	0.076 910	0.092 850	16.10	2.82	*WISE*
247195	2.847 924	0.120 740	0.261 754	15.90	2.98	*WISE*
248035 (†)	2.929 195	0.139 209	0.122 659	15.80	3.00	*WISE*
248581	2.920 784	0.100 786	0.076 717	15.70	3.20	*WISE*
249201	2.916 190	0.077 005	0.087 743	15.70	3.08	*WISE*
249283 (†)	2.894 856	0.105 884	0.214 428	16.10	2.72	*WISE*
250010 (†)	2.896 574	0.126 868	0.098 989	16.20	2.58	*WISE*
260891 (†)	2.945 898	0.111 076	0.172 986	15.80	3.22	*WISE*
261489	2.883 625	0.146 659	0.302 045	15.60	3.21	*WISE*
268622 (†)	2.858 875	0.075 933	0.127 763	16.20	2.58	*WISE*

likely the results of the formation of craters on Ceres larger than 300–400 km, should have been injected into the pristine region of the main belt. Collisional models predict that about 10 such craters could have formed on Ceres (Marchi et al. 2016). While the largest well-defined basins observed by Dawn on Ceres surface are smaller than 300 km, there is topographical evidence that larger impact structures formed in the ancient past (Marchi et al. 2016). The pristine region is characterized by a lower number density of asteroids, when compared to the central main belt. We argue that Ceres family members would be easier to recognize in this region, rather than near Ceres itself.

(iii) We analysed which objects in the pristine region have taxonomical, photometric, or albedo data comparable to that of Ceres. Remarkably, C-type candidates in this region cluster at inclinations that would be compatible with the range reached by possible Ceres' fragments. Among albedo C-type candidates, we observe a statistically significant peak in the $\sin(i)$ distribution at values close to that of Ceres itself. The number of C-type candidates at lower and higher inclinations is significantly lower, and no significant local sources can produce the observed distribution of C-type candidates.

While we believe that we have provided a circumstantial evidence in favour of a possible Ceres family in this work, we are aware that we have not proven its existence beyond any reasonable doubt. Since Ceres surface is characterized by a distinct 3μm absorption band (de Sanctis et al. 2015), observing this feature in some of the proposed Ceres family candidates could be a conclusive proof that such family exist, or existed in the past. Should the existence of a Ceres family be finally proved, future lines of research could investigate the possibility of some main belt comets (Hsieh 2015) being escaped members of this long-lost asteroid group.

REFERENCES

Beaugé C., Roig F., 2001, Icarus, 153, 391
Bendjoya P., Zappalà V., 2002, in Bottke W. F., Cellino A., Paolicchi P., Binzel R. P., eds, Asteroids III. Univ. of Arizona Press, Tucson, p. 613
Brasil P. I. O., Roig F., Nesvorný D., Carruba V., Aljbaae S., Huaman M. E., 2015, Icarus, 266, 142
Brož M., 1999, Thesis, Charles Univ., Prague, Czech Republic
Brož M., Morbidelli A., Bottke W. F., Rozenhal J., Vokrouhlický D., Nesvorný D., 2013, A&A, 551, A117
Brož M., Morbidelli A., 2013, Icarus, 223, 844
Bus J. S., Binzel R. P., 2002a, Icarus, 158, 106
Bus J. S., Binzel R. P., 2002b, Icarus, 158, 146
Carruba V., 2009, MNRAS, 395, 358
Carruba V., 2010, MNRAS, 408, 580
Carruba V., Machuca J. F., 2011, MNRAS, 418, 1102
Carruba V., Nesvorný D., 2016, MNRAS, 457, 1332
Carruba V., Burns J. A., Bottke W., Nesvorný D., 2003, Icarus, 162, 308

Carruba V., Huaman M. E., Domingos R. C., Santos C. R. D., Souami D., 2014, MNRAS, 439, 3168

Carruba V., Nesvorný D., Aljbaae S., Huaman M. E., 2015a, MNRAS, 451, 4763

Carruba V., Nesvorný D., Aljbaae S., Domingos R. C., Huaman M. E., 2015b, MNRAS, submitted

Carruba V., Nesvorný D., Aljbaae S., 2016, Icarus, 271, 57

de Sanctis M. C. et al., 2015, Nature, 528, 241

DeMeo F., Carry B., 2013, Icarus, 226, 723

Fu R., Ermakov A., Zuber M., Hager B., 2015, Union Fall Meeting. P23D-02: The Global Scale Relaxation State of Ceres. San Francisco

Hsieh H. H., 2015, preprint (arXiv:1511.01912)

Ivezić Ž. et al., 2001, AJ, 122, 2749

Knežević Z., Milani A., 2003, A&A, 403, 1165

Lazzaro D., Angeli C. A., Carvano J. M., Mothé-Diniz T., Duffard R., Florczak M., 2004, Icarus, 172, 179

Levison H. F., Duncan M. J., 1994, Icarus, 108, 18

Li J.-Y. et al., 2015, AAS/Division for Planetary Sciences Meeting Abstracts, 47, 103.04

Marchi S., Dell'Oro A., Paolicchi P., Barbieri C., 2001, A&A, 374, 1135

Marchi S. et al., 2013, Nat. Geosci., 6, 303

Marchi S. et al., 2016, Lunar Planet. Sci. Conf., Abstract #1281, Cratering on Ceres: The Puzzle of the Missing Large Craters

Masiero J. R., Mainzer A. K., Grav T., Bauer J. M., Jedicke R., 2012, ApJ, 759, 14

Milani A., Cellino A., Kneževicć Z., Novaković B., Spoto F., Paolicchi P., 2014, Icarus, 239, 46

Nathues A. et al., 2015, Nature, 528, 237

Nesvorny D., Broz M., Carruba V., 2015, in Michel P., De Meo F. E., Bottke W., eds, Asteroid IV, Univ. Arizona Press, Tucson, p. 297

Novaković B., Dell'Oro A., Cellino A., Knežević Z., 2012, MNRAS, 425, 338

Novaković B., Maurel C., Tsirvoulis G., Knežević Z., 2015, ApJ, 807, L5

Press V. H., Teukolsky S. A., Vetterlink W. T., Flannery B. P., 2001, Numerical Recipes in Fortran 77. Cambridge Univ. Press, Cambridge, p. 338

Rivkin A. S., Asphaug E., Bottke W. F., 2014, Icarus, 243, 429

Russell C. T. et al., 2012, Science, 336, 684

Russell C. T. et al., 2015, IAU General Assembly, 22, 2221738

Tholen D. J., 1989, in Binzel R. P., Gehrels T., Matthews M. S., eds, Asteroid III. University of Arizona Press, Tucson, p. 298

Vokrouhlický D., Brož M., Morbidelli A., Bottke W. F., Nesvorný D., Lazzaro D., Rivkin A. S., 2006, Icarus, 182, 92

This paper has been typeset from a TEX/LATEX file prepared by the author.